# Cellulose nanocrystal treatment of aligned short hemp fibre mats for reinforcement in polypropylene matrix composites

Sunny, Tom* and Pickering, Kim L.

School of Engineering, University of Waikato, Hamilton, 3240, New Zealand

* Corresponding author

Email: tomsunny54@gmail.com

**Abstract**

Oriented short hemp fibre mats were produced using dynamic sheet forming (DSF) incorporating cellulose nanocrystals (CNCs) to improve their integrity. The CNCs were found to act as a binder and improve mechanical strength of the mats as well as the strength of polypropylene matrix composites produced with the mats. Improved thermal stability was also obtained for composites by using CNC treatment of fibre mats.

**Keywords:** Cellulose Nanocrystals, Dynamic Sheet Forming, Compression Moulding.

## Introduction

The best tensile and flexural properties are generally obtained for fibre reinforced composites when the fibre is aligned parallel to the loading direction (Yu, Potter, and Wisnom 2014). However, the difficulty in getting alignment with short fibres makes randomly oriented fibre mats more common for natural plant fibre composites (Sunny, Pickering, and Lim 2017). Recent research has shown dynamic sheet forming (DSF), a method typically used in paper production, has the potential to produce aligned fibre mats and these mats could be successfully used in compression moulding with both thermoplastic and thermoset matrices (Le 2016). Composites with these fibre mats have exhibited higher mechanical performance compared to composites with random mats and other common short fibre composite manufacturing methods such as extrusion and injection moulding (Pickering, Efendy, and Le 2016).

The mechanical strength of the dried hemp fibre mats produced using DSF is weak as friction is the main force holding the loose hemp fibres together although there is potential for random fibre entanglement and limited hydrogen bonding (Fortea-Verdejo et al. 2016). The strength of the mats can be improved using methods such as needle punching or by spraying a polymer solution onto fibre mats, although this requires substantial infrastructure or use of solvents (Tekinalp et al. 2014).

An alternative method reported in the literature involves use of bacterial nanocellulose as a binder (Dai, Fan, and Collins 2013; Lee et al. 2012). Different approaches are being used by researchers to modify natural fibre surfaces with bacterial nanocellulose: culturing cellulose producing bacteria in the presence of natural fibres; dipping natural fibres in a suspension containing bacterial cellulose followed by vacuum filtration; and consolidation and drying to form the nonwoven mats. If successful, a basic spraying operation would offer greater potential for ease and improved time-effectiveness with in-line processing of mats. Although there are a few papers reporting the improvement of mechanical performance of fibre mats when treated with bacterial nanocellulose, as far as the authors are aware this is the first research to assess commercial grade nanocellulose treatment of aligned short fibre mats for reinforcement of composites.

## Experimental

### Materials

PP random copolymer SKRX3600, supplied by Clariant (New Zealand) Ltd with a melt index of 18g/10min and a density of 0.9 g/cm$^3$ was used as the matrix material. Maleic anhydride polypropylene (MAPP), grade A-C 950P, supplied by Honeywell International Inc., USA was

used as the coupling agent. Commercial grade cellulose nanocrystals (CNCs) that were provided as dry powder were purchased from Celluforce (Canada).

## Methods

Production of the fibre mats including alkali treatment of hemp fibres is detailed in a previous published work (Sunny, Pickering, and Lim 2020).

### *Cellulose nanocrystal treatment (CNC)*

Two CNC suspensions were investigated: one with 1 wt% CNCs and the other with 2 wt% CNCs in water. To prepare each CNC suspension, a predetermined amount of CNCs were added to distilled water and heated to 70 °C (Fig. 1a). The mixture was continuously stirred for half an hour using a magnetic stirrer, maintaining a temperature range of about 60 to 70 °C until it formed a homogeneous suspension. This suspension was then allowed to cool down to room temperature before being transferred into a small container. Application of the nanocellulose solution was carried out by spraying. Fig. 1b shows the spraying system used for the treatment. The set up involved support of the small container containing CNC suspension and a commercially available trigger spray attachment. Based on preliminary trials, the distance between the spray nozzle tip and the fibre mats was maintained at 450 mm to provide good coverage of the CNC suspension on the mats. Five spray applications were conducted on each side of the mat. After spraying on both sides, the mats were oven-dried for 3 h at 105 °C. This approach delivered 0.088 g (± 0.006) and 0.190 g (± 0.007) of CNCs onto the fibre mats with 1 (CNC1) and 2 wt% (CNC2) CNC treatments, respectively. After oven drying, the mats were stored in sealed polyethylene bags.

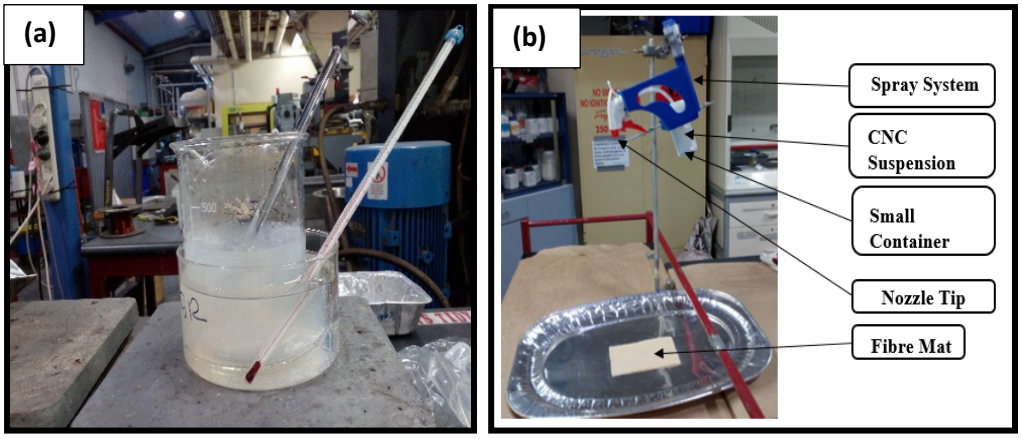


**Fig. 1 (**a) CNC solution preparation (b) CNC treatment

*Fourier transform infrared spectroscopy (FTIR)*

Fibre mat was ground to a fine power using a Retsch MM400 ball mill. All the samples were mixed and compressed with potassium bromide by applying a pressure of 8 tonnes/cm$^2$ to prepare sample discs for analysis. A PerkinElmer Spectrum One spectrometer was used to obtain infrared spectra of pure CNC, fibre mats without (CNC0) and with CNC treatments (CNC1, CNC2). A total of 20 scans were conducted for each sample in transmission mode from 4000 to 400 cm$^{-1}$.

*Raman spectroscopy*

The samples to be analysed were placed on aluminium foil and the laser power was set to 20 % of maximum. Raman spectra of pure CNC, fibre mats without (CNC0) and with CNC treatments (CNC1, CNC2) were acquired using a PerkinElmer RamanStation 400R spectrometer equipped with an air-cooled CCD detector. Each spectrum was acquired as the sum of five repeats of 20 s exposure on the same location on the sample.

*X-ray diffraction*

XRD spectra were obtained using an EMPYREAN diffractometer system (PANalytical) fitted with a Cu Kα X-ray tube. Fibre mats without (CNC0) and with CNC treatments (CNC1, CNC2)

were analysed. Crystallinity index ($I_c$ ) of the fibres was calculated using the Segal method (Segal et al. 1959).

*Production of PP/MAPP sheets*

PP blended with MAPP was formed into sheets using a Labtech 1201-LTE20-44 twin-screw extruder. The heating zones of the extruder barrel were set at 155 °C (feed entrance), 165 °C, 165 °C, 165 °C, 165 °C, 170 °C, 170 °C, 170 °C, 170 °C, 170 °C and 170 °C (at exit). The rotating screw speed was set to 45 rpm. The sheets produced were cut to 150 x 90 mm. In order to reduce the thickness of these polymer sheets, they were pressed between two aluminium plates inside a hot press. The average thicknesses of the sheets before and after pressing was 0.56 and 0.29 mm, respectively. The plates were lined with Teflon® sheets to avoid polymer sheets adhering to the plates. The time, applied pressure and temperature were 5 min, 1.5 MPa and 140 °C, respectively. After cooling down to room temperature, the polymer sheets were cut to the size of the mould (150 x 90 mm) used for the production of composites and stored in sealed bags.

*Fabrication of composite materials*

The fibre mats were weighed and arranged in a stack (Teflon sheets were used to prevent adhering of matrix material to the mould) with relative numbers of each according to the targeted fibre weight percentage. The stacks were then heated in a hot press at 170 °C for 5 minutes at 1 MPa). Table 1 represents the stacking arrangements and the abbreviations used for composites. It should be noted that the composites containing fibre content of about 25 wt% with 2 wt% CNC were heated at 170 °C for 5 minutes and pressed at 1 MPa (H25CNC2) or 2 MPa (H25CNC2$^{\#\#}$).

**Table 1** Abbreviations used for PP/MAPP and composite samples

| Samples | Targeted fibre wt% | Stacking arrangements | Thickness of polymer sheets used/mm | Production process of polymer sheets |
|---|---|---|---|---|
| PP/MAPP | - | 4PP* | 0.56 | Extrusion |
| H15CNC0<br>H15CNC1<br>H15CNC2 | 15 | 1PP*/1MAT/1PP*/1MAT/1PP*/1MAT/1PP* | 0.56 | Extrusion |
| H25CNC0#<br>H25CNC2#<br>H25CNC2## | 25 | 1PP*/1MAT/1PP*/1MAT/1PP*/1MAT/1PP*/1MAT/1PP*/1MAT/1PP* | 0.29 | Extrusion + Pressed between two aluminium sheets |
| H30CNC0<br>H30CNC1<br>H30CNC2 | 30 | 1PP*/3MATS/1PP*/3MATS/1PP* | 0.56 | Extrusion |
| H30CNC0#<br>H30CNC1#<br>H30CNC2# | | 1PP*/2MATS/1PP*/2MATS/1PP*/2MATS/1PP* | 0.29 | Extrusion + Pressed between two aluminium sheets |

**Note the following:** In the abbreviations, 'H' refers to hemp fibre and the number following 'H' is equal to the nominal weight percentage of fibres in composites. CNC0 = composites without CNC, CNC1 = composites with 1 wt% CNC treated fibre mats, CNC2 = composites with 2 wt% CNC treated fibre mats with polymer sheets of thickness 0.56 mm. # = composites made with polymer sheets of thickness 0.29 mm.

*Assessment of fibre mats and composites*

A Hitachi S-4700 scanning electron microscope, operated at 5 kV, was used to examine the surfaces of fibre mats and the fracture surfaces of composites. Prior to SEM observation, all samples were mounted on an aluminium stub using carbon tape and coated with platinum.

*Tensile testing of fibre mats and composites*

Prior to tensile testing, all samples were conditioned at 23 ± 1 °C and 50 % ± 2 % for 48 hours. The tensile testing of fibre mats was based on Tappi standard T 404 cm-92. An Instron-4204 universal testing machine fitted with a 10 N load cell and a crosshead speed of 1 mm/min was used for the testing. Ten strips of 150 x 20 mm were cut from the fibre mats in two directions, longitudinal and transverse to the rotation direction of DSF (fibre alignment direction). Tensile strengths for each direction were calculated as the breaking load divided by the width of the strip.

Procedures detailed in ASTM D 638-03; Standard Test Method for Tensile Properties of Plastics were followed for testing the composite specimens. An Instron-4204 universal testing machine fitted with a 5 kN load cell and an Instron 2630-112 extensometer with a gauge length of 50 mm was attached to the central part of the test specimen for the measurement of strain. The composite specimens were tested at a cross-head speed of 1 mm/min. A total of five samples were tested from each batch.

*Thermogravimetric analysis (TGA)*

Thermogravimetric analysis of the composites without CNC (H15CNC0) and with (H15CNC2) treatment was carried out using a PerkinElmer simultaneous thermal analyser STA 8000 instrument. A scanning range of 40 to 500 °C with a constant heating rate of 10 °C/min and airflow at 20 ml/min was used to obtain the data.

*Swelling studies*

Swelling studies were carried out to evaluate the interaction between the fibre and matrix in composites. The test was conducted according to the method reported in the literature with toluene as the solvent for immersion. (Ghazali and Efendy 2016). Samples with nominal dimensions of 30 x 5 x 3 mm were used and the dry weights (initial weights, w) of three replicate samples were measured. The samples were immersed in the solvent at room temperature for 48 hours and then taken out and wiped with a soft cloth. The weight of solvent absorbed was recorded and average values obtained. The swelling index of the composite is calculated using the following equation (John et al. 2008):

$$\text{Swelling Index}, \% = \frac{A_s}{w}\ x\ 100 \quad (1)$$

where $A_s$ = the amount of solvent absorbed.

**Results and Discussion**

Microscopic evaluation of fibre mats with and without CNCs

The surfaces of fibres with and without CNCs were observed by means of a scanning electron microscope (SEM). As can be seen in Fig. 2a, a large number of grooves appeared on the surfaces of fibres without CNC, as commonly seen in literature for alkali treated fibres (Pickering, Efendy, and Le 2016). Fig. 2b clearly shows the presence of rod-like CNCs on the fibre surfaces. It appears that a thin layer of CNCs films are covering the fibre surfaces. The CNCs deposited were measured using ImageJ software (Schneider, Rasband, and Eliceiri 2012) and were found to have average sizes of 15 (± 6.6) nm in width and 226 (± 66) nm in length. These dimensions are consistent with that previously reported for cellulose nanocrystals supplied from the manufacturer (Bardet et al. 2015). Strong interactions between CNCs and natural fibre surfaces are expected due to the affinity of cellulosic materials through hydrogen

bonding: a large number of hydroxyl groups available on the CNCs and the fibre surfaces promotes the potential for hydrogen bonding between them.

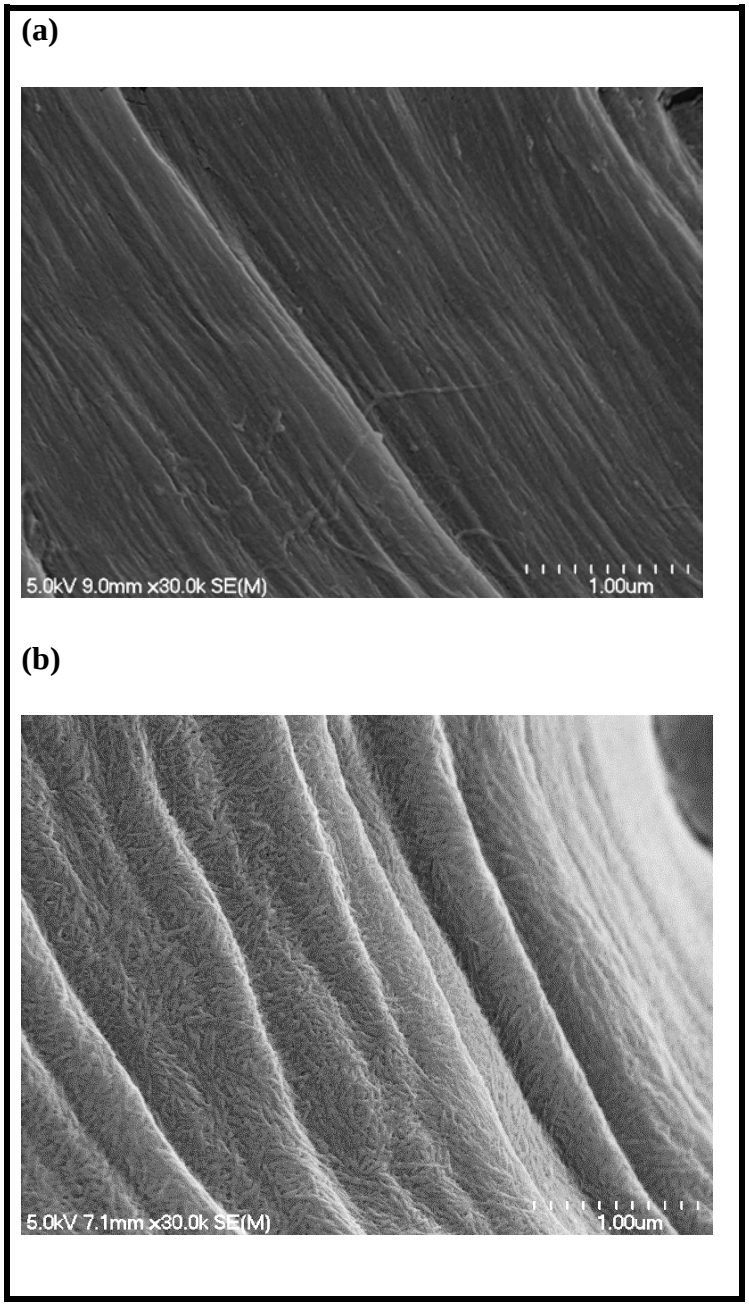


**Fig. 2** Scanning electron micrographs of fibre surfaces: (a) without CNC and (b) with CNC treatment

Fig. 3 shows the scanning electron micrographs of fibre mats without CNC (CNC0) and with CNC. The fibre mats without CNC appeared to have many gaps between the fibres (Fig. 3a). In

contrast, the fibre mats with CNCs appeared to have thin films formed between the fibres. Also, an increase in CNC content (from 1 to 2 wt%) was found to fill more gaps between the fibres (Fig. 3b compared to Fig. 3c). Generally, the films formed between the fibres within the mats indicated the potential of CNCs to act as binders and hold loose fibres together. There was also the indication of the self-organising capability (ability of CNCs to form as a film) of CNCs (Ross, Mayer, and Benziman 1991); films formed between the fibres consisted of several stacks of thin CNC films (Fig. 3e).

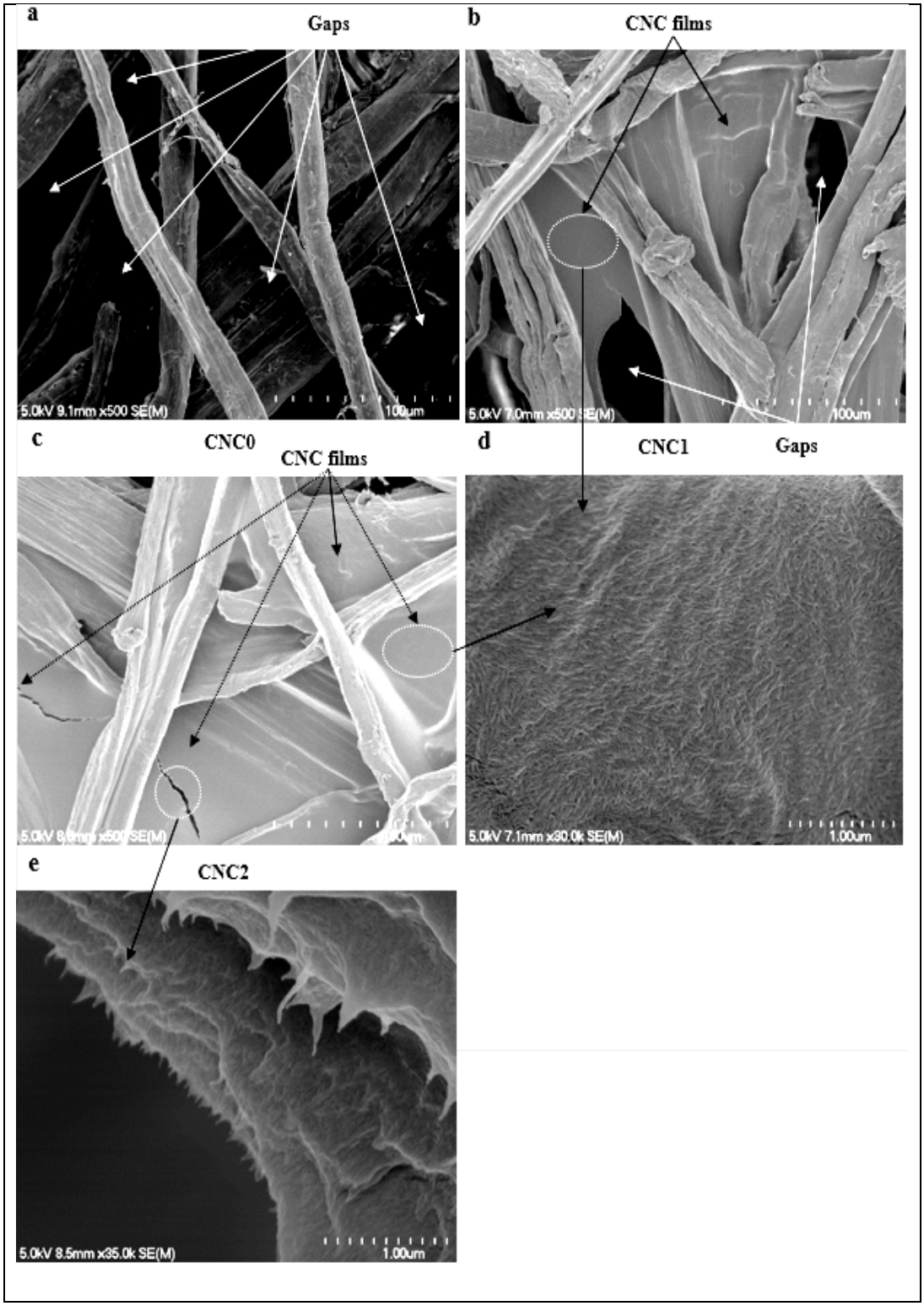


181

182 **Fig. 3** Scanning electron micrographs of fibre mats: (a)without CNC and (b,c,d,e) with CNC
183 (CNC1 and CNC2) treatments

184

The CNC was prepared from wood pulp by sulphuric acid hydrolysis (Bardet et al. 2015). It is well-known that sulphuric acid hydrolysis could have yielded CNCs with negatively charged surfaces, enabling them to disperse uniformly in water due to the electrostatic repulsions (Jordan, Easson, and Condon 2019). The fibre mats after treatment were oven dried at 105 °C for 3 hours. During the drying process, the evaporation of the suspending fluid (water) takes place, resulting in deposition of CNCs onto the fibre surfaces and formation of thin films between the fibres. It has been previously reported that the most notable property of CNCs is the ability to self-assemble and form as a film (Jativa et al. 2015). However, CNC was not expected in this research to form a uniform film throughout the mat as the CNC treatment was carried out by spraying.

Fourier transform infrared spectroscopy

Fourier transform infrared spectroscopic analysis was carried out to assess the chemical composition of pure CNC and fibre mats with and without CNC treatment. The spectra of the samples analysed are shown in Fig. 4. The region 3300-3400 $cm^{-1}$ in the spectra of all samples can be attributed to the stretching vibrations of the hydroxyl groups and reflects the hydrophilic nature of cellulosic materials (Chieng et al. 2017). The peak around 2900 $cm^{-1}$ corresponds to the stretching vibrations of C-H groups of cellulose (Gu et al. 2017). Although this peak appeared in the spectra of all samples, slightly higher peak intensity was shown for pure CNC compared to the fibre mats with or without CNC indicating the highly crystalline nature of pure CNCs. The peak at 1430 $cm^{-1}$ corresponds to the $CH_2$ bending vibration. The intensity of this peak appeared very sharp for the pure CNC followed by fibre mats with CNC treatment. It has been previously reported that the higher the intensity of this band, the higher the degree of crystallinity of the sample (Ciolacu, Ciolacu, and Popa 2011). The peaks around 1638 $cm^{-1}$ are commonly attributed to the bending vibration of hydroxyl groups (Das et al. 2018) and were present in the spectra of all samples. The peaks appearing in the range 1330-1360$cm^{-1}$ in the

spectra of all samples correspond to the bending vibrations of C-OH groups (Le Troedec et al. 2008). The peaks at 1238, 1058 and 896 $cm^{-1}$ are associated with the C-H groups bending, C-H stretching and bending vibrations of cellulose (Alemdar and Sain 2008). These peaks were present in the spectra of all samples. The 1058 peak appeared in the range 900-1500 $cm^{-1}$ and was very strong for pure CNC followed by the fibre mats with CNC and then without CNC. These results strongly indicate the presence of high crystalline CNCs on the fibre mats.

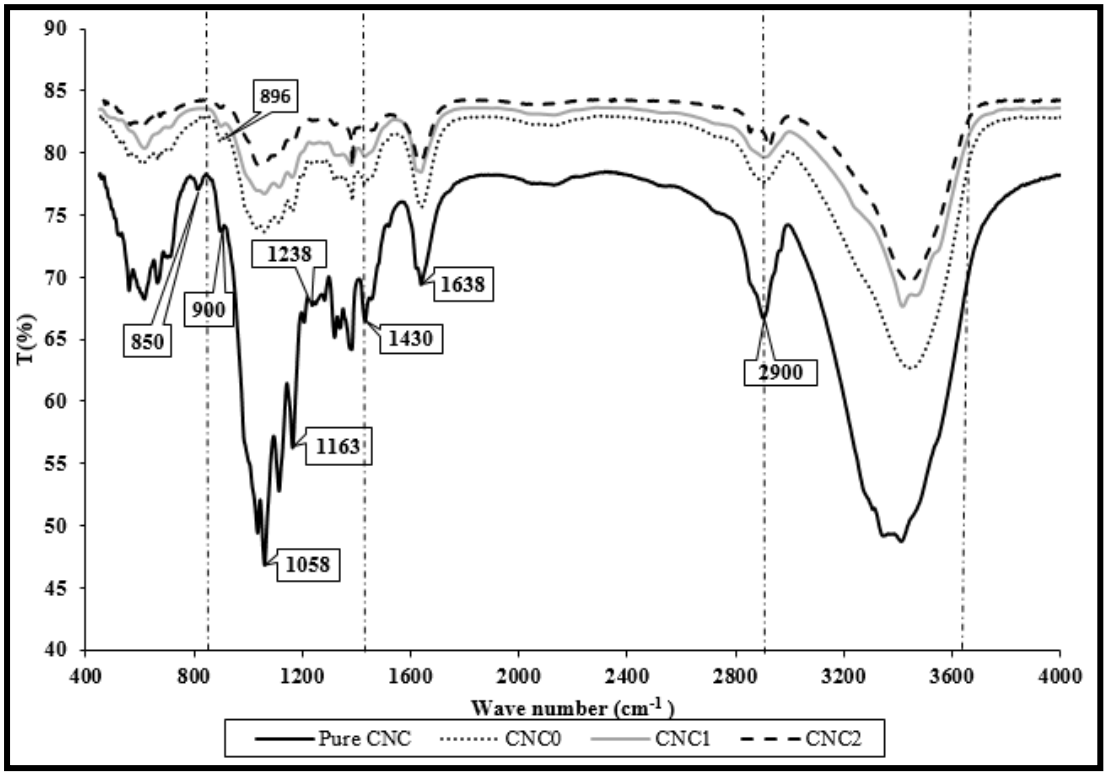


**Fig. 4** FTIR spectra of fibre mats without (CNC0) and with CNC treatments (CNC1 and CNC2) and pure CNC

The strong peaks at 850 $cm^{-1}$ and 1163 $cm^{-1}$ in the spectrum of pure CNC indicate the presence of sulphate groups ($SO_2$ groups). The formation of sulphate ester groups as a result of sulphuric acid hydrolysis has been previously reported (Niu et al. 2017). It is well known that the presence of $SO_2$ groups reduce the thermal stability of CNC (Wei et al. 2014). The disappearance of this peak from the spectra of CNC treated fibre mats indicates that the fibre mats are free of sulphate groups. This could be due to oven drying of the mats at 105 °C for 3

h (Bardet et al. 2015). It has been previously reported that oven drying at 105 °C for only 5 min removed 75 % of sulphur content from CNC films as a result of desulphation (the loss of negatively charged sulphate ester groups and their replacement by OH groups) (Beck and Bouchard 2014).

Raman analysis

Raman analysis was carried out mainly to confirm the removal of sulphate groups from the spectra of CNC treated fibre mats. Raman spectra of pure CNC, the fibre mats with and without CNC treatments can be seen in Fig. 5. When compared to the fibre mats without CNC treatment, the intensity of cellulose peaks at 1098 $cm^{-1}$, 1120 $cm^{-1}$, 1374 $cm^{-1}$ and 2900 $cm^{-1}$ appeared sharper for pure CNCs and fibre mats with CNC treatments, supporting the presence of CNCs on the fibre mats (Agarwal 2017). In the region between 1500 and 2500 $cm^{-1}$ there appeared no evidence of peaks for cellulose in the Raman spectra. A similar observation has been previously reported (Szymanska-Chargot, Cybulska, and Zdunek 2011). The characteristic peaks associated with the S-S bond of sulphur appeared in the range 400-500 $cm^{-1}$ in the spectrum of pure CNC confirming the presence of $SO_2$ groups in CNCs (Xu et al. 2016). The absence of these peaks from the spectra of CNC treated fibre mats indicated the removal or reduction of sulphate groups of CNCs. Also, the peaks in the range 1050-1200 $cm^{-1}$ related to $SO_2$ groups appeared very weak or absent in the spectra of CNC treated fibre mats and further supports that the fibre mats were mostly free of $SO_2$ groups (Börjesson et al. 2018).

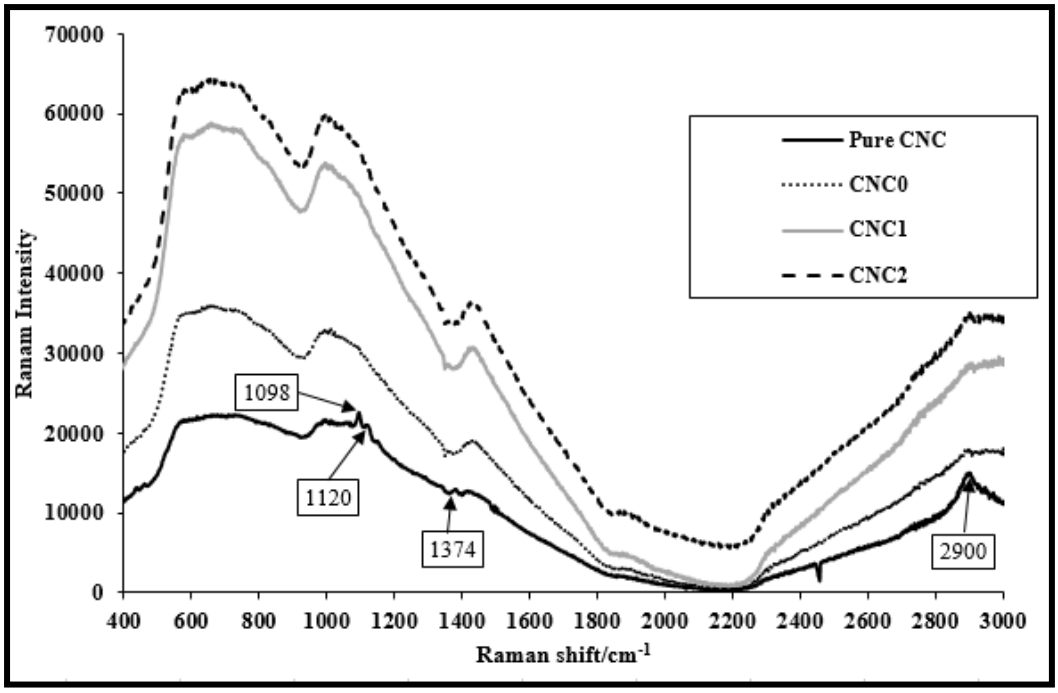


**Fig. 5** Raman spectra of fibre mats without and with CNC treatments and pure CNC

Overall, the combination of FTIR and Raman spectroscopy results indicated that the CNC treated fibre mats were largely free of sulphur groups or these techniques were not able to detect the sulphate groups due to the very low levels present.

Cellulose crystallinity index ($I_c$)

The major peaks for crystalline phases of most cellulosic fibres are generally observed at about $2\theta$ = 15, 17, 22.7 and 35 ° (denoted as 'a', 'b', 'c' and 'd', respectively) as shown in Fig. 6, representing the (110), $(1\bar{1}0)$, (200) and (004) crystallographic planes, respectively for cellulose I (Beckermann 2007) . As expected, the major crystalline peak (200) of cellulose for the fibre mats with or without CNC treatments appeared at about $2\theta$ = 22.7 °. In order to calculate the crystallinity index, the intensity of diffraction of the amorphous material ($I_{am}$) was taken at $2\theta$ = 18.3 ° (denoted as 'e' in Fig. 6), where the intensity is minimum. It should be noted that the crystallinity index is commonly considered for comparison instead of describing absolute crystallinity (Islam, Pickering, and Foreman 2011). As can be seen in the results

presented in Table 2, the crystallinity index of the fibre mats increased with CNC treatment. Such behaviour is expected with the applied treatment, as highly crystalline CNCs are deposited onto the fibre surfaces.

**Table 2** Crystallinity index ($I_c$) of hemp fibres without and with CNC treatments

| Samples | $I_{am}$ (18.3 °) | $I_{200}$ (22.7 °) | Crystallinity index (%) |
|---|---|---|---|
| CNC0 | 1963 | 255 | 87 |
| CNC1 | 2086 | 181 | 91 |
| CNC2 | 3664 | 290 | 92 |

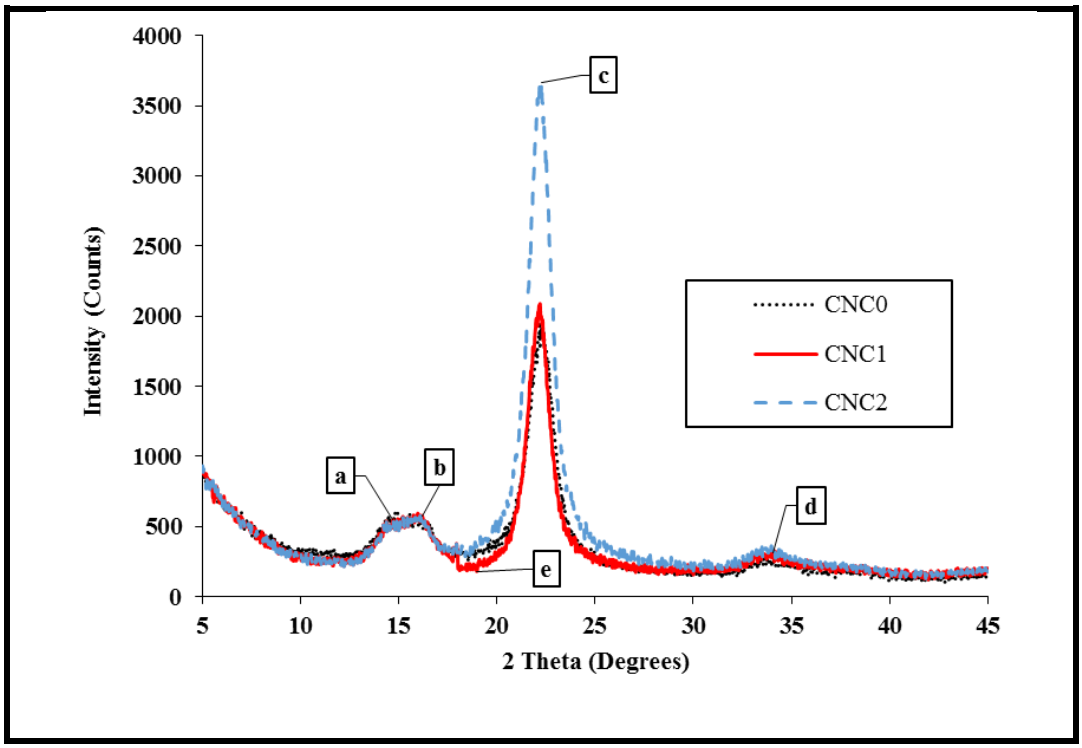


**Fig. 6** X-ray diffraction curves of fibre mats without and with CNC treatments used in calculating crystallinity index ($I_c$)

Fibre mat assessment

Although attempts were made to obtain the tensile strength of the fibre mats without CNC and with 1 wt% CNC, they were very weak with strength below the accuracy limits of the equipment. Table 3 displays the average tensile strengths and the ratio of transverse tensile

strength to longitudinal obtained for the 2 wt% CNC treated fibre mats. The strength was calculated by dividing the maximum load required to break the mat by its width, as the cross-section area of the fibre mats is not well defined. Improved strength with 2 wt% CNC supports that the CNC could act as a binder. It has been previously reported that the ratio between transverse tensile strength (TTS) to the longitudinal tensile strength (LTS) indicates the degree of fibre orientation (Le 2016). The ratio TTS/LTS for the fibre mats was 0.39 (± 0.27).

**Table 3** Tensile strengths of fibre mats with 2 wt% CNC treatment

| LTS (kN/m) | TTS (kN/m) | TTS/LTS |
|---|---|---|
| 0.11 (± 0.04) | 0.03 (± 0.02) | 0.39 (± 0.27) |

**Note:** LTS: longitudinal tensile strength, TTS: transverse tensile strength. Values in parentheses are the standard deviations

The weight percentage gains in fibre mats with respect to the CNC treatments are shown in Fig. 7. The maximum weight gain was found to be approximately 4 wt% when treated with 2 wt% CNC solution.

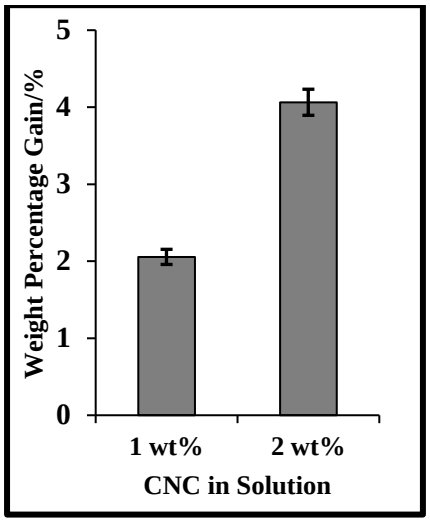


**Fig. 7** Weight percentage gain in the fibre mats with respect to the CNC treatment

291 Tensile properties of composites

292 The average tensile strengths of composites and the matrix only (PP/MAPP) samples are
293 represented in Fig. 8a. The composite tensile strengths were normalised by the weight
294 percentage of fibre as shown in Fig. 8b. Tensile strengths of all composites were higher than
295 that of the matrix only material (Fig. 8a). At a fibre content of 15 wt%, the average tensile
296 strength of composites with 1 and 2 wt% CNC treated fibre mats increased from 14.8 to 23.6
297 and 26.5 MPa, respectively, compared to the matrix only material; these were approximately
298 2.1 and 14.8 % higher than the respective composites without CNC treated fibre mats. However,
299 the increase of composite tensile strength was only found to be statistically significant
300 (Student's t-test) with the inclusion of 2 wt% CNC treated fibre mats. The normalised graph
301 (Fig. 8b) was used to ensure that the increases in composite tensile strength were due to CNC
302 addition and not due to variability in the precise fibre content. The improvement in composite
303 tensile strength with CNC treated fibre mats is thought to be due to the addition of high strength
304 nanocellulose. It has previously been reported that the introduction of high strength and high
305 modulus nanocellulose into composites could enhance the tensile strength and Young's
306 modulus of the composites (Ng et al. 2015).

307

308

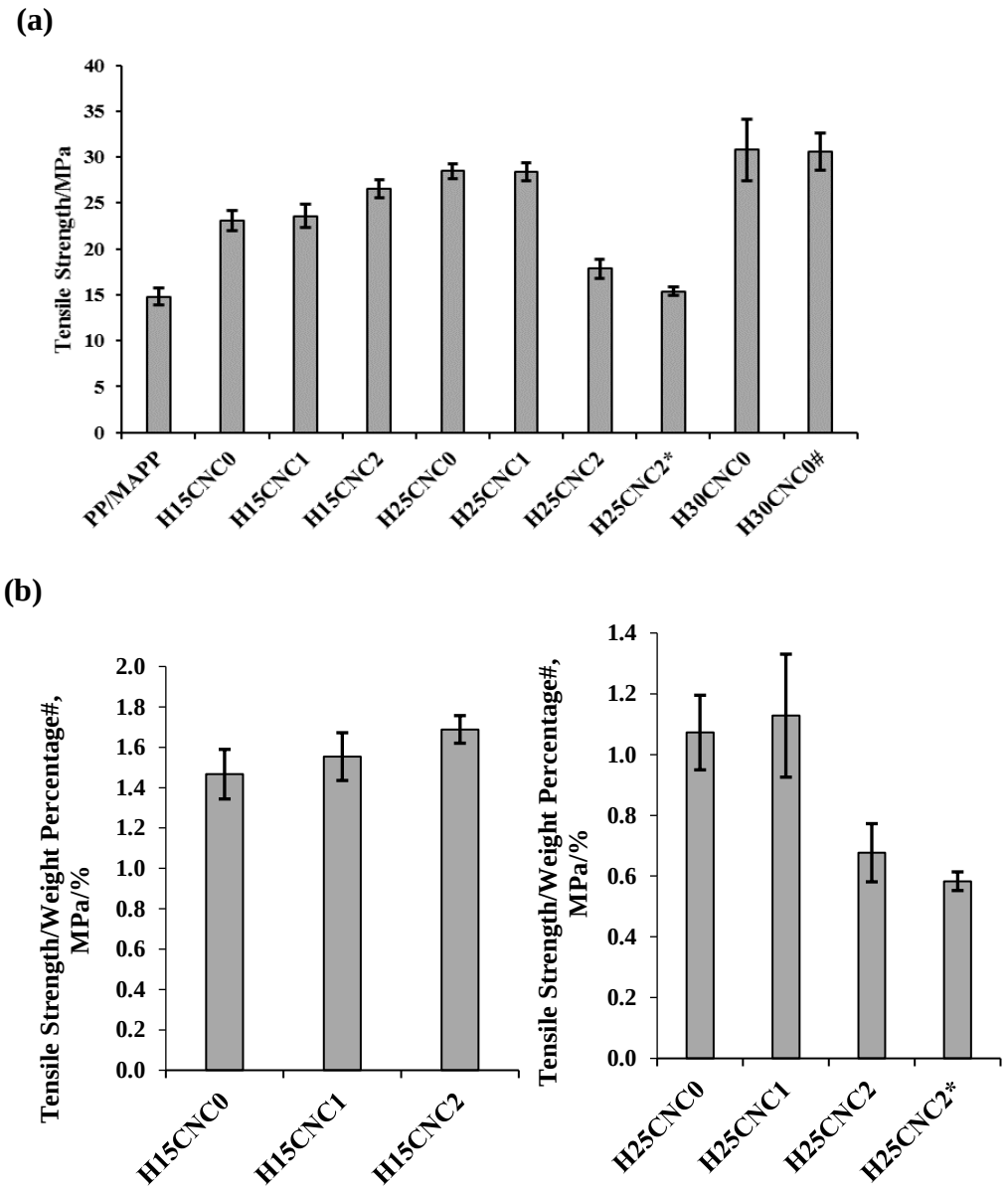


**Fig. 8** (a) Average tensile strengths of PP/MAPP and various composites (b) Average tensile strength/weight percentage[#] of fibres in composites. # = weight percentage of fibre with CNC content (normalised). Note the following: composites were approximately 15, 25 and 30 wt%

In the absence of CNCs, an increase in fibre content significantly increased the composite tensile strength (c.f PP/MAPP, H15CNC0, H25CNC0 and H30CNC0). Little difference was observed for the addition of 1wt% CNC. However, the incorporation of 2 wt% CNC treated fibre mats was found to significantly decrease the composite tensile strength when the fibre content increased from 15 to 25 wt %. Decreases of composite tensile strength when there is a higher 34 CNC content, compared to the composites without CNCs, is due to the poor fibre

wetting by the matrix. This indicates that the CNC films formed among the fibres (see Fig. 2) within the mats most likely acted as a barrier to the matrix. A further decrease in the tensile strengths for the composites was observed with the increase in the amount of pressure applied during compression moulding due to the breakage of fibre mats: 1 MPa to 2 MPa (H25CNC2 compared to H25CNC2[*]). No reliable data was acquired for the tensile strength of composites containing CNCs (for either 1 and 2 wt%) with a fibre content of 30 wt% due to poor consolidation (see Fig. 9). Among the composites, the highest tensile strength was achieved by the composites with a fibre content of 30 wt% (H30CNC0 and H30CNC0[#]) regardless of the thickness of polymer sheets (0.56 or 0.29 mm).

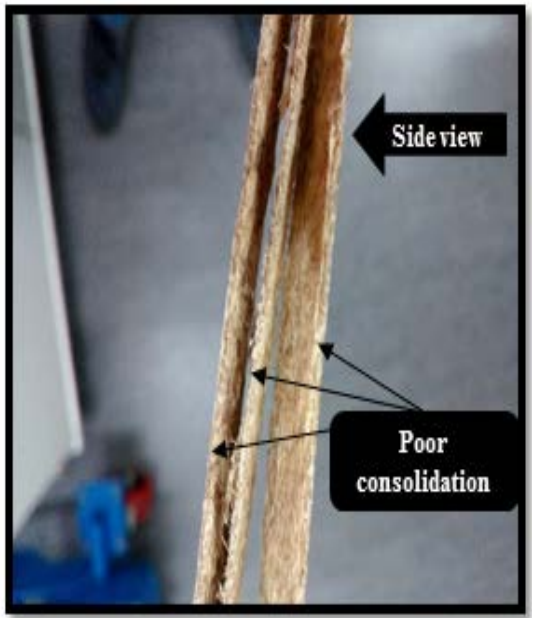


**Fig. 9** A side cross-section image of 30 wt% composite with CNC sample (cut-edge) displaying poor consolidation

The average Young's modulii of various composites and the control (PP/MAPP) samples are represented in Fig. 10a. Similar to tensile strengths for the composites, a normalised graph (Fig. 10b) was used to ensure whether there was any change in Young's modulus for composites due to CNC addition and not due to variability in the precise fibre content. A similar trend to that of composite tensile strengths was observed. When compared to composites without CNC, an

increase by about 16 % was noticed for the composites with 2 wt% CNC and fibre content of 15 wt%, supporting interfacial adhesions between the CNC treated fibre mats and the PP/MAPP matrix. Fig. 11 shows the stress-strain curves for the composites with and without CNC treatments. The stiffness of the composites appears to increase with increasing CNC contents, although the failure strains decreased.

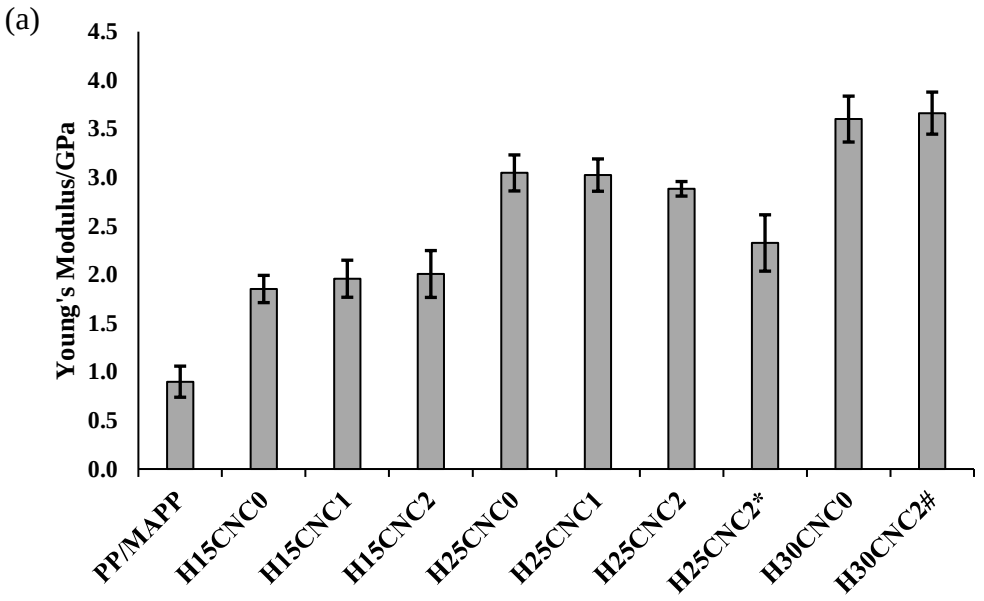


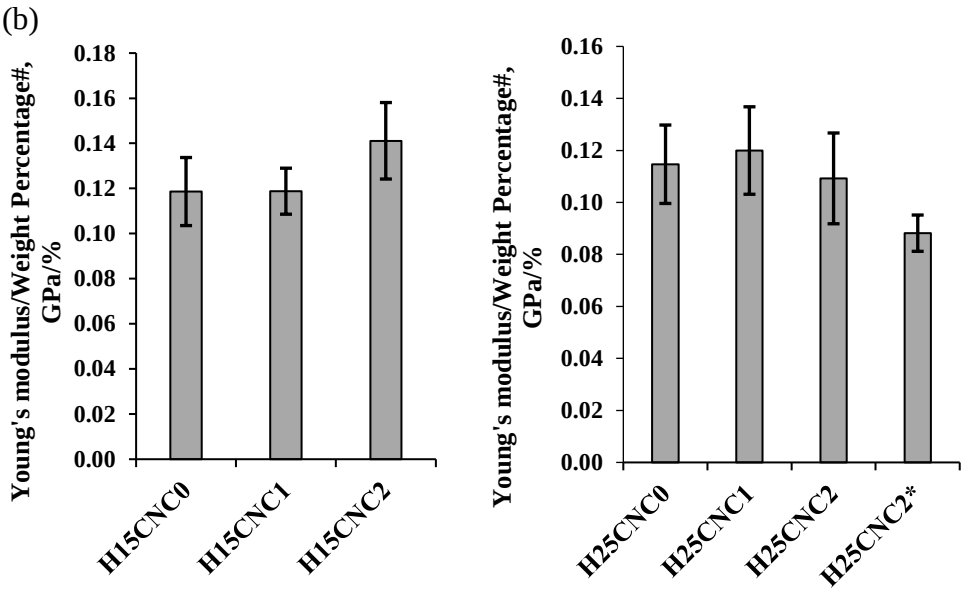

**Fig. 10** (a) Average Young's modulus of PP/MAPP and various composites (b) Young's modulus/weight percentage[#] of fibres in composites (normalised). # = weight percentage of fibre with CNC content

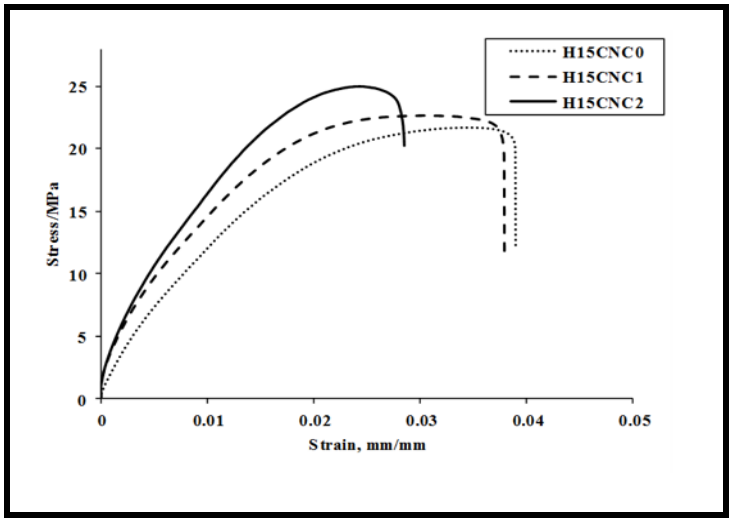


**Fig. 11** Stress-strain curves of 15 wt% composites with and without CNC treated fibre mats

The scanning electron micrographs of the tensile fracture surfaces of composites without and with CNC treated fibre mats can be seen in Fig. 12a to 12f. The fracture surfaces of the 15 wt% composites with CNC treated fibre mats appeared rougher compared to those composites without CNC treated fibre mats (Fig. 12b, 12c and 12e compared to Fig. 12a and 12d). This could be an indication that the addition of CNCs had improved the fibre-matrix interfacial adhesion or at least the interfacial surface area. It has previously been reported that the failure mode for composites, where there is increased interfacial bonding is more like matrix and fibre tearing (Heng et al. 2012). However, composites with high fibre and CNC contents appeared to have very poor fibre wetting (Fig. 12f), suggesting that the CNC films formed between the fibres acted as a barrier and restricted the flow of the molten polymer through the composites. It is well known that for the formation of good interfacial adhesion between the fibres and matrix in a composite, the molten matrix material should ideally flow around and fully wet the fibres. Poor fibre wetting results in weak fibre-matrix interfaces with defects such as fibre pull-out and voids, which act as stress raisers, thus reducing the overall mechanical performance of composites (Juntaro et al. 2012).

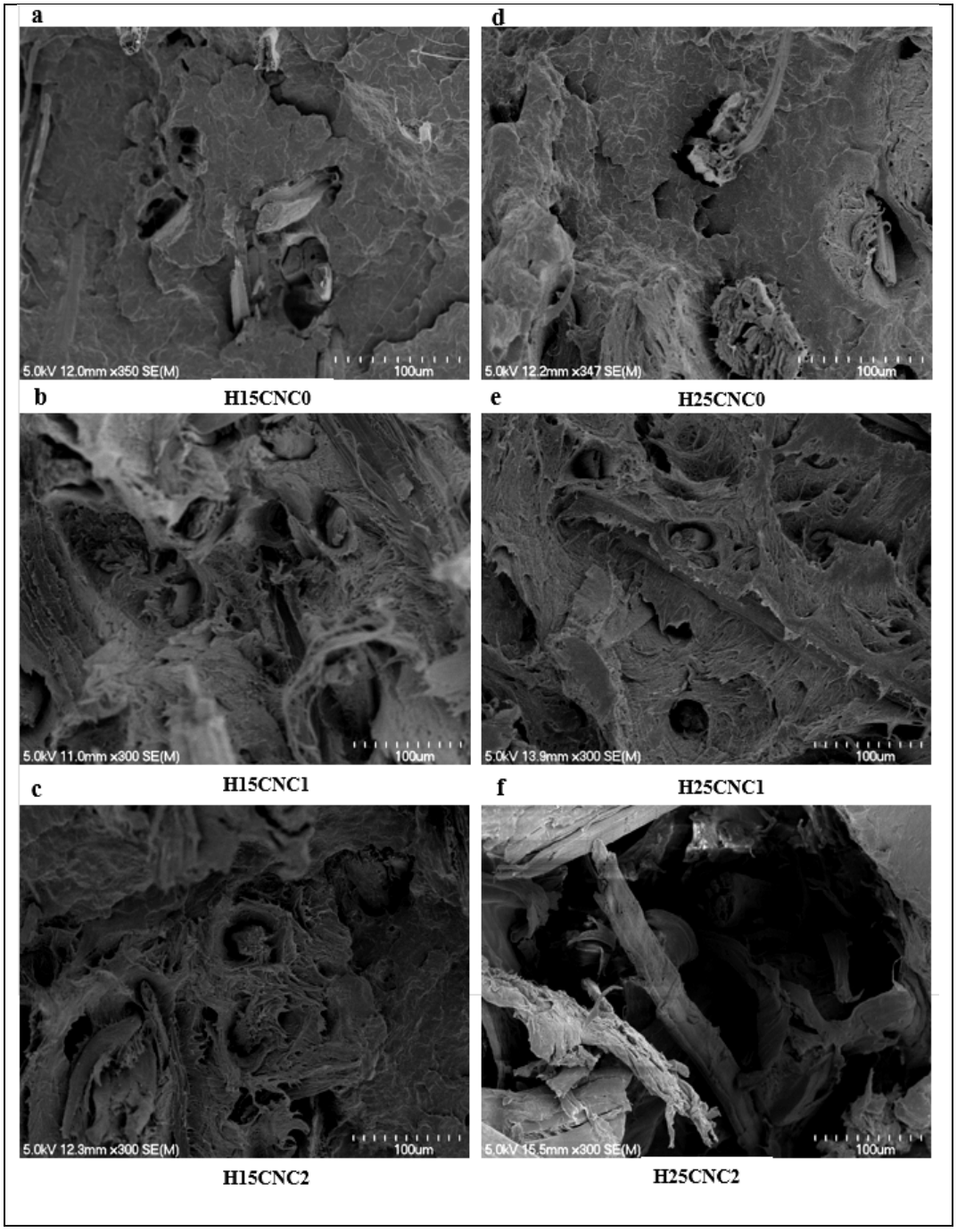


**Fig. 12** Scanning electron micrographs of tensile fracture surfaces of composites: (a,d) without CNC and (b,c,e,f) with CNC treated fibre mats. Note the following: In the abbreviations, 'H' refers to hemp fibre and the number following 'H' is equal to the nominal weight percentage of fibres in composites. CNC0 = composites without CNC, CNC1 = composites with 1 wt% CNC treated fibre mats, CNC2 = composites with 2 wt% CNC treated fibre mats

Thermogravimetric analysis (TGA)

Thermogravimetric curves for composites with and without CNC are shown in Fig. 13. Both composites started losing mass around 260 °C. Above 260 °C up to a temperature of 360 °C,

371 an increase in thermal stability for the composites with CNC was observed. This apparent
372 increase in the thermal stability of the composites is likely to be due to improved interfacial
373 bonding due to the addition of CNCs, as described in the literature (Ragoubi et al. 2012).

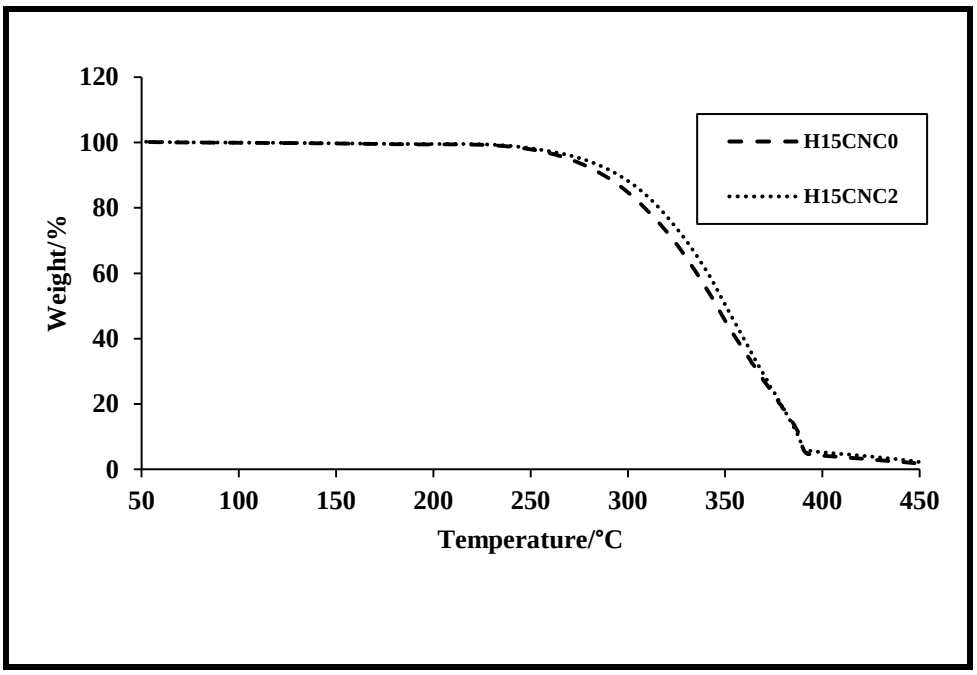


374 **Fig. 13** TGA curves for composites with and without CNC treated fibre mats (heating rate of
375 10 °C/min and airflow at 20 ml/min)
376

377 Swelling studies

378 As can be seen in Fig. 14, the composites with 2 wt% CNC treated fibre mats had the lowest
379 swelling indices. This further indicates that the presence of CNCs improved the interfacial
380 adhesion for composites with 15wt% fibre between the treated fibre mats and the PP/MAPP
381 matrix. It has previously been reported that the coating of natural fibres with nanocellulose
382 increases the surface area of the fibres due to its highly crystalline nature, thus resulting in
383 improved fibre wetting with polymer materials (Papirer et al. 2000; Heng et al. 2012).

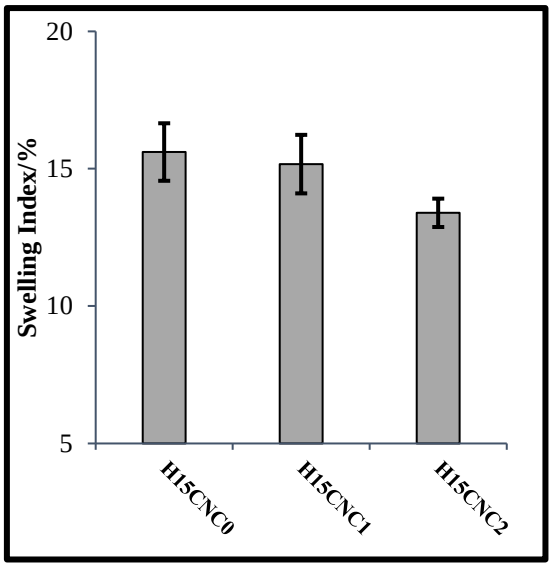


**Fig. 14** Swelling indices for hemp composites. Samples were immersed for 48 h

## Conclusions

This investigation has shown that cellulose nanocrystals can be sprayed onto the fibre mats to help bind fibres together. The fibre mats possessed an average tensile strength of about 0.11 $kNm^{-1}$ when treated with 2 wt% CNCs in water, whereas those mats treated with 1 wt% and without CNCs possess no measurable tensile strength using a 10 N load cell. It appeared that the addition of CNCs modified the fibre surfaces (CNC coating) as well as filled the gaps between the fibres within the mats (thin CNC films). The addition of 2 wt% CNC in 15 wt% composites brought about increases of 15 and 16 % in tensile strength and Young's modulus, respectively.This indicates that the CNC addition improved the fibre-matrix interfacial adhesion. The lower swelling indices and higher thermal stability obtained for the composites with CNC treated fibre mats compared to those composites without CNC treated fibre mats also supports the improved interfacial bonding in composites with the addition of CNC. At low fibre content, the production method of composites with CNC treated fibre mats by compression moulding was found to be effective and resulted in a good consolidated final product. However, at high fibre contents, the composites with CNC displayed very poor

consolidation. The CNC films formed between the fibres are most likely acting as barriers, restricting the flow of the molten polymer through the composites resulting in poor fibre wetting and reduction in tensile strength and Young's modulus of these composites. More research needs to be carried out to further explore the spray pressure and flow rate of the spraying process.

## Declarations

This research received no specific grants from any agency in the public, commercial, or not-for-profit sectors. However, the authors would like to thank the University of Waikato's composite research group for their support. The authors declare that there is no conflict of interest. Ethical approval was not required for this study.

## Reference

Agarwal, Umesh P (2017) Raman spectroscopy of CNC-and CNF-based nanocomposites. Handbook of Nanocellulose and Cellulose Nanocomposites 18:609-25.

Alemdar, A., and M. Sain (2008) Isolation and characterization of nanofibers from agricultural residues: wheat straw and soy hulls. Bioresour Technol 99:1664-71. https://www.ncbi.nlm.nih.gov/pubmed/17566731.

Bardet, R., F. Roussel, S. Coindeau, N. Belgacem, and J. Bras (2015) Engineered pigments based on iridescent cellulose nanocrystal films. Carbohydr Polym 122:367-75. https://www.ncbi.nlm.nih.gov/pubmed/25817681.

Beck, Stephanie, and Jean Bouchard (2014) Auto-catalyzed acidic desulfation of cellulose nanocrystals. Nord Pulp Pap Res J 29:6-14. https://doi.org/10.3183/npprj-2014-29-01-p006-014.

Beckermann, Gareth. 2007. 'Performance of Hemp-Fibre Reinforced Polypropylene Composite Materials', Doctoral, University of Waikato.

Börjesson, Mikaela, Karin Sahlin, Diana Bernin, and Gunnar Westman (2018) Increased thermal stability of nanocellulose composites by functionalization of the sulfate groups on cellulose nanocrystals with azetidinium ions. Journal of Applied Polymer Science 135:45963. https://doi.org/10.1002/app.45963.

Chieng, B. W., S. H. Lee, N. A. Ibrahim, Y. Y. Then, and Y. Y. Loo (2017) Isolation and Characterization of Cellulose Nanocrystals from Oil Palm Mesocarp Fiber. Polymers (Basel) 9:355. https://www.ncbi.nlm.nih.gov/pubmed/30971032.

Ciolacu, Diana, Florin Ciolacu, and Valentin I Popa (2011) Amorphous cellulose—structure and characterization. Cellul Chem Technol 45:13.

Dai, Dasong, Mizi Fan, and Philip Collins (2013) Fabrication of nanocelluloses from hemp fibers and their application for the reinforcement of hemp fibers. Industrial Crops and Products 44:192-99. https://doi.org/10.1016/j.indcrop.2012.11.010.

Das, Debabrata, Shamima Hussain, Anup Kumar Ghosh, and Arun Kumar Pal (2018) STUDIES ON CELLULOSE NANOCRYSTALS EXTRACTED FROM MUSA SAPIENTUM: STRUCTURAL AND BONDING ASPECTS. Cellul Chem Technol 52:729-39.

Fortea-Verdejo, Marta, Koon-Yang Lee, Tanja Zimmermann, and Alexander Bismarck (2016) Upgrading flax nonwovens: Nanocellulose as binder to produce rigid and robust flax fibre preforms. Composites Part A: Applied Science and Manufacturing 83:63-71. https://doi.org/10.1016/j.compositesa.2015.11.021.

Ghazali, Mohd, and Aruan Efendy. 2016. 'Bio-composites materials from engineered natural fibres for structural applications', University of Waikato.

Gu, J., C. Hu, R. Zhong, D. Tu, H. Yun, W. Zhang, and S. Y. Leu (2017) Isolation of cellulose nanocrystals from medium density fiberboards. Carbohydr Polym 167:70-78. https://www.ncbi.nlm.nih.gov/pubmed/28433179.

Heng, Jerry Y. Y., Duncan F. Pearse, Frank Thielmann, Thomas Lampke, and Alexander Bismarck (2012) Methods to determine surface energies of natural fibres: a review. Composite Interfaces 14:581-604. https://doi.org/10.1163/156855407782106492.

Islam, Mohammad S., Kim L. Pickering, and Nic J. Foreman (2011) Influence of alkali fiber treatment and fiber processing on the mechanical properties of hemp/epoxy composites. Journal of Applied Polymer Science 119:3696-707. https://doi.org/10.1002/app.31335.

Jativa, F., C. Schutz, L. Bergstrom, X. Zhang, and B. Wicklein (2015) Confined self-assembly of cellulose nanocrystals in a shrinking droplet. Soft Matter 11:5374-80. https://www.ncbi.nlm.nih.gov/pubmed/26059700.

John, Maya Jacob, Bejoy Francis, K. T. Varughese, and Sabu Thomas (2008) Effect of chemical modification on properties of hybrid fiber biocomposites. Composites Part A: Applied Science and Manufacturing 39:352-63. https://doi.org/10.1016/j.compositesa.2007.10.002.

Jordan, J. H., M. W. Easson, and B. D. Condon (2019) Alkali Hydrolysis of Sulfated Cellulose Nanocrystals: Optimization of Reaction Conditions and Tailored Surface Charge. Nanomaterials (Basel) 9:1232. https://www.ncbi.nlm.nih.gov/pubmed/31480286.

Juntaro, Julasak, Marion Pommet, Athanasios Mantalaris, Milo Shaffer, and Alexander Bismarck (2012) Nanocellulose enhanced interfaces in truly green unidirectional fibre reinforced composites. Composite Interfaces 14:753-62. https://doi.org/10.1163/156855407782106573.

Le, Tan Minh. 2016. 'Harakeke fibre as reinforcement in epoxy matrix composites and its hybridisation with hemp fibre', University of Waikato.

Le Troedec, Marianne, David Sedan, Claire Peyratout, Jean Pierre Bonnet, Agnès Smith, René Guinebretiere, Vincent Gloaguen, and Pierre Krausz (2008) Influence of various chemical treatments on the composition and structure of hemp fibres. Composites Part A: Applied Science and Manufacturing 39:514-22. https://doi.org/10.1016/j.compositesa.2007.12.001.

Lee, Koon-Yang, Kingsley K. C. Ho, Kerstin Schlufter, and Alexander Bismarck (2012) Hierarchical composites reinforced with robust short sisal fibre preforms utilising bacterial cellulose as binder. Composites Science and Technology 72:1479-86. https://doi.org/10.1016/j.compscitech.2012.06.014.

Ng, Hon-Meng, Lee Tin Sin, Tiam-Ting Tee, Soo-Tueen Bee, David Hui, Chong-Yu Low, and A. R. Rahmat (2015) Extraction of cellulose nanocrystals from plant sources for application as reinforcing agent in polymers. Composites Part B: Engineering 75:176-200. https://doi.org/10.1016/j.compositesb.2015.01.008.

Niu, F., M. Li, Q. Huang, X. Zhang, W. Pan, J. Yang, and J. Li (2017) The characteristic and dispersion stability of nanocellulose produced by mixed acid hydrolysis and ultrasonic assistance. Carbohydr Polym 165:197-204. https://www.ncbi.nlm.nih.gov/pubmed/28363540.

Papirer, E., E. Brendle, H. Balard, and C. Vergelati (2000) Inverse gas chromatography investigation of the surface properties of cellulose. Journal of Adhesion Science and Technology 14:321-37. https://doi.org/10.1163/156856100742627.

Pickering, K. L., M. G. Aruan Efendy, and T. M. Le (2016) A review of recent developments in natural fibre composites and their mechanical performance. Composites Part A: Applied Science and Manufacturing 83:98-112. https://doi.org/10.1016/j.compositesa.2015.08.038.

Ragoubi, M., B. George, S. Molina, D. Bienaimé, A. Merlin, J. M. Hiver, and A. Dahoun (2012) Effect of corona discharge treatment on mechanical and thermal properties of composites based on miscanthus fibres and polylactic acid or polypropylene matrix. Composites Part A: Applied Science and Manufacturing 43:675-85. https://doi.org/10.1016/j.compositesa.2011.12.025.

Ross, P., R. Mayer, and M. Benziman (1991) Cellulose biosynthesis and function in bacteria. Microbiol Rev 55:35-58. https://www.ncbi.nlm.nih.gov/pubmed/2030672.

Schneider, C. A., W. S. Rasband, and K. W. Eliceiri (2012) NIH Image to ImageJ: 25 years of image analysis. Nat Methods 9:671-5. https://www.ncbi.nlm.nih.gov/pubmed/22930834.

Segal, LGJMA, J Jr Creely, AE Martin Jr, and CM Conrad (1959) An empirical method for estimating the degree of crystallinity of native cellulose using the X-ray diffractometer. Textile research journal 29:786-94. https://doi.org/10.1177/004051755902901003.

Sunny, Tom, Kim L Pickering, and Shen Hin Lim. 2017. "Alignment of Short Fibres: An Overview." In *Processing and Fabrication of Advanced Materials-XXV*, 616-25.

Sunny, Tom, Kim L. Pickering, and Shen Hin Lim (2020) Alkali treatment of hemp fibres for the production of aligned hemp fibre mats for composite reinforcement. Cellulose 27:2569-82. https://doi.org/10.1007/s10570-019-02939-3.

Szymanska-Chargot, M., J. Cybulska, and A. Zdunek (2011) Sensing the structural differences in cellulose from apple and bacterial cell wall materials by Raman and FT-IR spectroscopy. Sensors (Basel) 11:5543-60. https://www.ncbi.nlm.nih.gov/pubmed/22163913.

Tekinalp, Halil L., Vlastimil Kunc, Gregorio M. Velez-Garcia, Chad E. Duty, Lonnie J. Love, Amit K. Naskar, Craig A. Blue, and Soydan Ozcan (2014) Highly oriented carbon fiber–polymer composites via additive manufacturing. Composites Science and Technology 105:144-50. https://doi.org/10.1016/j.compscitech.2014.10.009.

Wei, B., X. Xu, Z. Jin, and Y. Tian (2014) Surface chemical compositions and dispersity of starch nanocrystals formed by sulfuric and hydrochloric acid hydrolysis. PLoS One 9:e86024. https://www.ncbi.nlm.nih.gov/pubmed/24586246.

Xu, Jing, Dawei Su, Wenxue Zhang, Weizhai Bao, and Guoxiu Wang (2016) A nitrogen–sulfur co-doped porous graphene matrix as a sulfur immobilizer for high performance lithium–sulfur batteries. Journal of Materials Chemistry A 4:17381-93. https://doi.org/10.1039/C6TA05878G.

Yu, H., K. D. Potter, and M. R. Wisnom (2014) A novel manufacturing method for aligned discontinuous fibre composites (High Performance-Discontinuous Fibre method). Composites Part A: Applied Science and Manufacturing 65:175-85. https://doi.org/10.1016/j.compositesa.2014.06.005.